Supporting information

Synergistically Interactive MnFeM (M=Cu, Ti, and Co) Sites Porous g-C_3N_4 Fiber-like Nanostructures for an Enhanced Green Hydrogen Production

Belal Salah[a,b‡], Ahmed Abdelgawad[a,b‡], Qingqing Lu[c], Adewale K. Ipadeola[a,b], Rafael Luque[d,e], and Kamel Eid[a]*

a. Gas Processing Center, College of Engineering, Qatar University, Doha 2713, Qatar.
b. Center for advanced materials, Qatar University, Doha 2713, Qatar
c. Engineering & Technology Center of Electrochemistry, School of Chemistry and Chemical Engineering, Qilu University of Technology (Shandong Academy of Sciences), Jinan, China.
d. Peoples Friendship University of Russia (RUDN University), 6 Miklukho Maklaya str., 117198, Moscow, Russian Federation
e. Universidad ECOTEC, Km 13.5 Samborondón, Samborondón, EC092302, Ecuador.
‡ Contributed equally to this work.
**Corresponding author E-mail: kamel.eid@qu.edu.qa*

Experimental

Chemicals and Materials

Copper (II) chloride (($CuCl_2.2H_2O$), 99.99 %), cobalt (II) chloride (($CoCl_2.2H_2O$), 99.99 %), (melamine, 99 %), manganese (II) chloride monohydrate ($MnCl_2{\cdot}H_2O$), Iron (II) chloride tetrahydrate ($FeCl_2{\cdot}4H_2O$), titanium (IV) isopropoxide $Ti[OCH(CH_3)_2]_4$, ethanol solution ((CH_3CH_2-OH), 99.8 %), nitric acid ((HNO_3), 70 %), and commercial Pt/C catalyst (10 wt.% Pt) were purchased from Sigma-Aldrich Chemie GmbH.

Synthesis of MnFeCu/g-C_3N_4

Porous MnFeCu/g-C_3N_4 fiber-like nanostructures were synthesized based on our previous report but with changing reaction parameters and conditions along with utilizing ultrasonic treatment[1, 2]. This includes a dispersion of melamine (4 g) in an aqueous solution of ethanol (200 mL), $MnCl_2.2H_2O$ (2mL, 10 mM), $FeCl_2.4H_2O$ (2mL, 10 mM), and $CuCl_2.2H_2O$ (2mL,10 mM) via ultrasonic treatment for 10 min. This is followed by slow addition of 60 mL HNO_3 (0.1 M) and then left under magnetic stirring for 1 h. Finally, the obtained precipitate was filtrated and washed with ethanol/H_2O (3/1 v/v) for 4 times and dried at 100 °C for 2 h. The obtained powder was annealed at 550 °C (10° /min, 5°/min heating rate) for 2 h under N_2.

This method was also used to prepare porous MnFeTi/gC_3N_4 and MnFeCo/g-C_3N_4 fiber-like nanostructures, but with the replacement of $CuCl_2.2H_2O$ with $Ti[OCH(CH_3)_2]_4$ and $CoCl_2.2H_2O$, respectively.

Metal-free g-C_3N_4 was formed using the same method, but without metal precursors.

Materials Characterization

The scanning electron microscope ((SEM), Hitachi S-4800, Hitachi, Tokyo, Japan)) and the transmission electron microscope ((TEM), TecnaiG220, FEI, Hillsboro, OR, USA), equipped with high-angle annular dark-field scanning transmission electron microscopy (HAADF-SEM), and energy dispersive spectrometer (EDX) was used for investigation of the morphology and composition. The X-ray photoelectron spectroscopy (XPS) spectra were recorded on a Thermo ESCALAB 250 spectrometer, while the X-ray diffraction spectra were measured on an X-ray diffractometer (X'Pert-Pro MPD, PANalytical Co.). The inductively coupled plasma optical emission spectrometry (ICP-OES, Agilent 5800) was used for elemental composition.

Electrochemical HER

The cyclic voltammogram (CVs), linear sweep voltammogram (LSV), electrochemical impedance spectroscopy (EIS), and chronoamperometry (CA) tests were measured on Gamry potentiostat (Reference 3000, Gamry Co., Warminster, PA, USA). This is using a three-electrode cell of Pt wire (3 mm) as a counter electrode, Ag/AgCl as a reference electrode, and glassy carbon electrode (GCE) ((⌀5 mm x 1 mm) as a working electrode. The GCE was initially polished with 0.3 and 0.05 μm of alumina slurry and then rinsed by double deionized H_2O three times under sonication, followed by deposition the 10-20 μl catalyst ink (2mg/mL in isopropanol/H_2O/Nafion (5 wt.%) (4/1/0.05 v/v/v) on the working electrodes through volumetric casting and then left to dry under vacuum at 80 °C. The metal loading (i.e. Pt or MnFeM) of each catalyst on the GCE was adjusted to 0.004 mg_{metal} /cm^2 based on the ICP-OES data. The obtained HER currents were corrected against Ohmic potential drop, and the potentials were normalized to the reversible hydrogen electrode (RHE) using equation (Eqn. 1).

$$E_{RHE} = E_{Ag/AgCl} + 0.197\ V + 0.059 \times pH \quad \text{(Eqn. 1)}$$

The mass activity (MA) was calculated at 0.4V using the following equation (Eqn. 2)

$MA=J_{HER}/M$ (Eqn. 2)

Where J_{HER} is the HER current density, and M is the metal (Pt or MnFeM) loading on the GCE.

The specific activity (SA) was calculated at 0.4V using the following equation (Eqn. 3)

$SA=J_{HER}/MxECSA$ (Eqn. 3)

Where ECSA is the electrochemical active surface.

The turnover frequency (TOF) was calculated using the following equation (Eqn. 4)

$TOF = (J_{HER} \times F) / (n \times A)$ (Eqn. 4)

Where F is the Faraday constant (96,485 C/mol), n is the number of electrons transferred per H_2, and A is the surface area of the catalyst.

Table S1. Comparison of the hydrogen production (electrocatalytic and/or photocatalytic) of carbon nitride-based nanostructured catalysts with literature

Catalyst	**Preparation Method**	**Metal dopants**	**Metal Loading (Wt.%)**	**Morphology of CN**	**Catalytic reaction**	**Electrolyte**	**HER rate ($\mu mol \cdot g^{-1} \cdot h^{-1}$) /overpotential (mV)**	**Ref.**
MnFeCu/gCN MnFeTi/gCN MnFeCo/gCN MnFe/gCN Mn/gCN	Protonation by HNO_3 (0.1 M, 60 mL) in ethanol (200 mL) under ultrasonic treatment and annealing (550 °C/2h)	Mn, Fe, Cu, Ti, Co	2.0 - 2.3	Porous fiber-like	Electrocatalytic HER	H_2SO_4	3774.35/ 400 1902.54/ 548 1820.10/ 564 2110.64/ 475 872.20/ 583	This work
PtPd/CNs	Protonation by $NaNO_3$ (0.1 M) and HCl (0.1 M) in Ethylene glycol (15 mL) and annealing (550 °C/2h)	Pt. Pd	1.5	Nanorods	Electrochemical and photoelectrochemical CO oxidation	-	-	[3]
Pd/CN NWs Pd-Cu/CN-NWs	Protonation by HNO_3 (0.2 M, 60 mL) in ethanol (30 mL) and annealing (400 °C/2h)	Pd, Cu	1.2 0.6-0.6	Nanowires Nanowires	Thermal CO oxidation	-	-	[4]
Au/Pd/gC_3N_4 NTs	Protonation by HNO_3 (0.1 M, 70 mL) in ethylene glycol (30 mL) and annealing (450 °C/2h)	Pd, Au	0.5-0.5	Nanotubes	Thermal CO oxidation	-	-	[5]
Pd/gC_3N_4NTs Cu/gC_3N_4NTs Pd/Cu/gC_3N_4-NTs	Protonation by HNO_3 (0.1 M 60 mL)) in Ethylene glycol (30 mL) and annealing (550 °C/2h)	Pd, Cu	1.1 1.1 0.55-0.55	Nanotubes Nanotubes Nanotubes	Thermal CO oxidation	-	-	[2]
Pd/gC_3N_4NFs Au/gC_3N_4NFs Au/Pd/gC_3N_4 NFs	Protonation by HNO_3 (0.3 M, 60 mL) in isopropanol (30 mL) and annealing (480 °C/2h)	Pd, Au	1 1 0.5-0.5	Nanofibers Nanofibers Nanofibers	Thermal CO oxidation	-	-	[1]
Cu/P-g-C_3N_4	Protonation of Melamine and pyridine by HNO_3 (0.2 M, 20 mL) in 1,2-ethanediol (50 mL) and annealing (550 °C/2h)	Cu	1.8	hierarchical porous crumpled nanosheets	Thermal CO oxidation	-	-	[6]
Cu/g-C_3N_4 Mn/g-C_3N_4 Fe/g-C_3N_4	Protonation by HNO_3 (0.1 M, 20 mL) in ethanol (100 mL) and annealing at (550	Cu, Mn, Fe	1.7 ±0.2	Fiber-like	Electrochemical HER	0.5 M H_2SO_4	222.15/ 449 91.15/ 610 110.80/ 560	[7]

	°C/2h)							
Pt/CCTs	Sonication, freeze-drying, and calcined (550 °C/3h)	Pt	3	Nanotubes	Photocatalytic HER	0.2 M Na_2SO_4 + TEOA	3538.30/-	[8]
Pt/HR-CN	Nanocasting template, calcined (550 °C/4h) and etching, Pt/HR-CN by in-situ photodeposition of Pt	Pt	3	Helical nanorods	Photocatalytic HER	0.01 M $AgNO_3$ + TEOA + acetonitrile	74 µmol/h/ -	[9]
Pt/CN-MU	Thermal condensation of melamine and urea (1:10) (400 °C/4h) then anneaing at 550 °C for 4h	Pt	0.5	Holey nanotubes	Photocatalytic HER	0.5 M Na_2SO_4 + 20 vol.% lactic acid	1073.60/ -	[10]
TiO_2/g-CN	TiO_2 by hydrothermal at (150 °C/4h) and calcination (500 °C/1hr) then TiO_2/g-CN by solvothermal (180 °C/24h) and calcination (520 °C/1h)	Ti	-	Nanorod arrays	Photoelectrochemical HER	0.2 M Na_2SO_4	- / 160	[11]
TiO_2/P-C_3N_4/Co_3O_4	TiO_2 by hydrothermal (180 °C/4h), impregnated in cyanuric acid and diammonium hydrogen phosphate solution, calcination(550 °C/2h), immersed in Co solution reduced by NaOH, calcination (350 °C/3h)	Co, Ti	-	Nano dot Core-nanorod shell	Photoelectrochemical HER	0.5 M Na_2SO_4	26.16 $\mu mol \cdot cm^{-1} \cdot h^{-1}$/ 920	[12]
MoS_2/g-C_3N_4	g-C_3N_4 by Hydrothermal/calcination (180/4hr, 600 °C/4h), MoS_2 by hydrothermal (200 °C/24h), and MoS_2/g-C_3N_4 by mixed impergnation	Mo	10-30	Nanoflake/nanotube	Photocatalytic HER	0.5 M Na_2SO_4	1124.00/ -	[13]
PtNi/g-C_3N_4	g-C_3N_4 by calcination (600 °C/3h) and PtNi/g-C_3N_4 by co-reduction using $NaBH_4$ (0.05 M)	Pt, Ni	0.99	Nanotubes	Photocatalytic HER	0.2 M Na_2SO_4	104.8 µmol h^{-1} / -	[14]
Ni_2P-$Cd_{0.9}Zn_{0.1}S$/g-C_3N_4	Ni_2P-$Cd_{0.9}Zn_{0.1}S$ by two-step Hydrothermal (220 °C/24hr, 200 °C/24h), g-C_3N_4 by calcination(550 °C/4h) and Ni_2P-$Cd_{0.9}Zn_{0.1}S$/g-C_3N_4 by self-assembly for 24h	Ni, Cd, Zn	0.5-6.0	Nanorods	Photocatalytic HER	0.15 M Na_2S + 0.05 Na_2SO_4	121.20 µmol mg^{-1} h^{-1}/-	[15]
1D-RuO_2-CN_x	CN_x by Microwave irradiation(180 °C/3h), and 1D-RuO_2-CN_x by hydrothermal reduction by ($NaBH_4$/120 °C/8h), then hydrothermal treatment (350 °C/12h)	Ru	24.41	Nanowires	Electrocatalytic HER	0.5 M H_2SO_4 0.5 M KOH	- / 93 - / 95	[16]
g-C_3N_4 nanoribbon-G	GO by Hummers method, g-C_3N_4 by calcination (600 °C/2h), and chemically treated/ g-C_3N_4 nanoribbon-G by Hydrothermal treatment (180 °C/6h)	-	-	Nanoribbon	Electrocatalytic HER	0.5 M H_2SO_4	-/ 207	[17]

PtCo/$Na_{0.1}$SCNNT	$Na_{0.1}$SCNNT by precursor mixing, grinding, and thermal polymerization / PtCo/$Na_{0.1}$SCNNT by chemical reduction	Pt, Co, Na	1.38-2.38	Nanotubes	Photocatalytic HER	0.2 M Na_2SO_4 + 10 vol.% TEOA	254.70 µmol h^{-1}	[18]
T-CN	Annealing (450 °C/4h) Mixture of Melamine with (KCl, LiCl) molten salt assisted	Pt	3	Hollow tubes	Photocatalytic HER	0.1 M Na_2SO_4 + 10 vol.% TEOA	332.00/ -	[19]
TCN-0.1	Thermal polymerization (Urea, MF resin mixture) (600 °C/3h)	Pt	3	Multistage tubular	Photocatalytic HER	0.2 M Na_2SO_4 + 10 vol.% TEOA	7505.00/ -	[20]
g-CNNTs(540)	Unidirectional freezing of urea, annealing at (540 °C/2h)	Pt	3	Hollow tubes	Photocatalytic HER	0.2 M Na_2SO_4 + 10 vol.% TEOA	8789/-	[21]
CN-10	Solvothermal polymerization (180 °C/12h) and calcination (550 °C4h)	Pt	3	Spongelike fibers	Photocatalytic HER	0.5 M Na_2SO_4 + 10 vol.% TEOA	2227.00/ -	[22]
R-TCNT	Hydrothermal of spherical melamine (180 °C/8h) and annealing (500 °C/4h)	-	-	Bunchy microtubes	Photocatalytic HER	0.5 M Na_2SO_4 + 10 vol.% TEOA	8.19 µmol h^{-1}/ -	[23]
P-TCN/GQDs-0.15	P-TCN by hydrothermal and calcination (180 °C/4h, 500 °C/10h), and P-TCN/GQDs by Lyophilization method	-	-	Hexagonal Tubular	Photocatalytic HER	0.1 M Na_2SO_4	112.10 µmol h^{-1}/ -	[24]
Pt/PCNC	Two-step (Hydrothermal self-assembly/ Self-template, 200 °C/12h) pyrolysis(550 °C/3h)	Pt	3	Coral-like architecture	Photocatalytic HER	0.1 M Na_2SO_4 + 10 vol.% TEOA	5289.90/ -	[25]
Pt/P-TCN	Hydrothermal (180 °C/10h) and heat treatment (500 °C/4h), and Pt/P-TCN in-situ photodeposition of pt precursor	Pt	1	Rod-like	Photocatalytic HER	0.1 M Na_2SO_4	67.00 µmol h^{-1}/ -	[26]
Pt/g-C_3N_4	Hydrothermal (200 °C/12h) and pyrolysis (550 °C/4h) and Pt/g-C_3N_4 in-situ photodeposition of pt precursor	Pt	3	Nanotubes	Photocatalytic HER	10 vol.% TEOA	118.50 µmol h^{-1}/ -	[27]
Pt/CN-OA-0.03	CN-OA-0.03 by facial wet chemistry and annealing (550 °C/2h) and Pt/CN-OA-0.03 by in-situ photodeposition of pt precursor	Pt	3	Nanotubes	Photocatalytic HER	10 vol.% TEOA	12.60 µmol h^{-1}/ -	[28]
Ag-Cu(3)C_3N_4 NTs 1:1	C_3N_4 by multistep (calcination (550 °C/2h), exfoliation, heating 350 °C, rapid cooling in ice) and Ag-Cu(3)C_3N_4 NTs by metals chemical reduction	Ag, Cu	3-5	Nanotubes	Photocatalytic HER	0.01 M Na_2SO_4 + 10 vol.% TEA, TEOA and MeOH	738.00 µmol g^{-1}/ -	[29]
Pt/CNS-550	Calcination (550 °C/2h), Recrystallization in acidic(H_2SO_4/methanol mixture)	Pt	3	Nanotubes	Photocatalytic HER	0.1 M Na_2SO_4 + 10 vol.%	261.80 µmol h^{-1}/ -	[30]

	and annealing (550 °C/2h) and Pt/CNS-550 by in-situ photodeposition of pt precursor					TEOA		
Ba-P-CN	Hydrothermal (180 °C/10h) and calcination (500 °C/4h)	Pt	3	Microtube	Photocatalytic HER	0.25 M Na_2SO_4 + 17 vol.% TEOA	12.30 µmol h^{-1}/ -	[31]
Pt/GCN-THP	calcination (550 °C/4h, (Ar, CCl_4)), then LP-CNP rinsed by water and calcenied (500 °C/2h)	Pt	3	Tetragonal hollow prism	Photocatalytic HER	0.5 M Na_2SO_4 + 10 vol.% TEOA	1990.00/ -	[32]
Pt/CN-SP	Hydrothermal (180 °C/10h) and annealing (500 °C/4h)	Pt	1	Hexagonal tube stacked nanosheets	Photocatalytic HER	0.2 M Na_2SO_4 + MeOH	57.00 µmol h^{-1}/ -	[33]
Pt/3wt%NaCl-CN	hydrothermal (200 °C/12h) and Thermal condensation (550 °C/2h) and Pt by in-situ photo-deposition	Pt	1	Nanowires	Photocatalytic HER	0.25 M Na_2SO_4 + 17 vol.% TEOA	4.95 µmol h^{-1}/ -	[34]
Pt/I/N-CN	Hydrothermal (180 °C/10h) and annealing (500 °C/4h) and Pt loaded by photodeposition	Pt	3	nanotubes	Photocatalytic HER	0.5 M Na_2SO_4 + 17 vol.% TEOA	9.75 µmol h^{-1}/ -	[35]
Pt/MCN	halloysite as templet annealed (850 °C/2h) and activated by HCl (80 °C/6h), then melamine deposited on activated halloysite by vapor deposition (520 °C/4h), then templet etched by HF	Pt	3	Wormlike nanorods	Photocatalytic HER	10 vol.% TEOA	633.00/ -	[36]
HGCNF/SNG/ MoS_2	Electrospinning and sintering method at (580 °C/ 4h) followed by autoclave for hydrothermal treatment at	Mo	10.26	Hollow nanofibers	Electrocatalytic HER	0.5 M H_2SO_4	- / 282	[37]
Pt(3.0wt%)M o_2C/g-C_3N_4	freeze-dried (-50 °C/48h) then annealed (800 °C/ 4 h)	Pt, Mo	4	Rod-like	Photocatalytic HER	0.5 M Na_2SO_4 + 10 vol.% TEOA	507.00/ -	[38]
Pt/O-g-C_3N_4	Thermal condensation (500 °C/2h) and Pt loaded by photodeposition	Pt	3	Nanorods	Photocatalytic HER	0.5 M Na_2SO_4 + 15 vol.% TEOA	732.00/ -	[39]
Rh/77CNNb	Molten salt and thermal condensation (520 °C/4hr)	Rh, Sr, Nb	0.91-1.8	Nanorods	Photocatalytic HER	-	0.183 h^{-1}/ -	[40]

Carbon quantum dots implanted g-C3N4 nanotubes (CCTs); g-C3N4 with a helical rod-like morphology (HR-CN); CN from melamine and urea in a 1:1 (CN-MU); carbon nitride nanotube (CNNT); triethanolamine (TEOA); Bundle thins carbon nitride tubes (R-TCNT); tubular carbon nitride (TCN), graphene quantum dot (GQD); porous bionic coral-like architecture (PCNC); phosphorus-doped hexagonal tubular carbon nitride (P-TCN); triethylamine (TEA); graphitic carbon nitride tetragonal hollow prism (GCN-THP); methanol (MeOH); C3N4- modified sodium pyrophosphate (CN-SP); mesoporous g-C3N4 nanotubes (MCN); hollow g-C3N4 nanofibers (HGCNF); sulfur/nitrogen-doped graphene (SNG); g-C3N4/Sr2KNb5O15 with 77 wt.% of g-C3N4 (77CNNb)

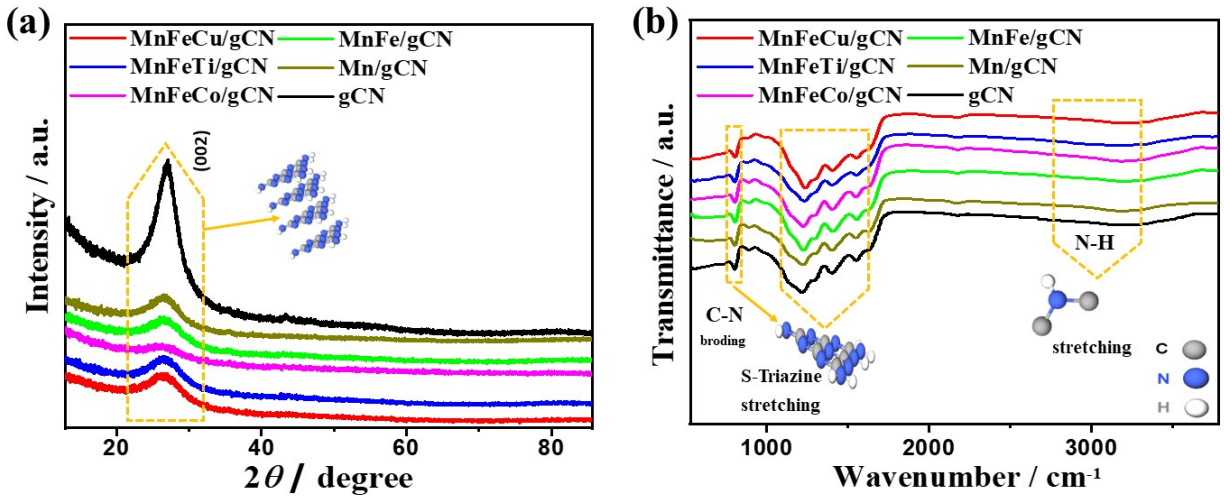

Figure S1. (a) XRD analysis and (b) FTIR spectra of thus obtained materials

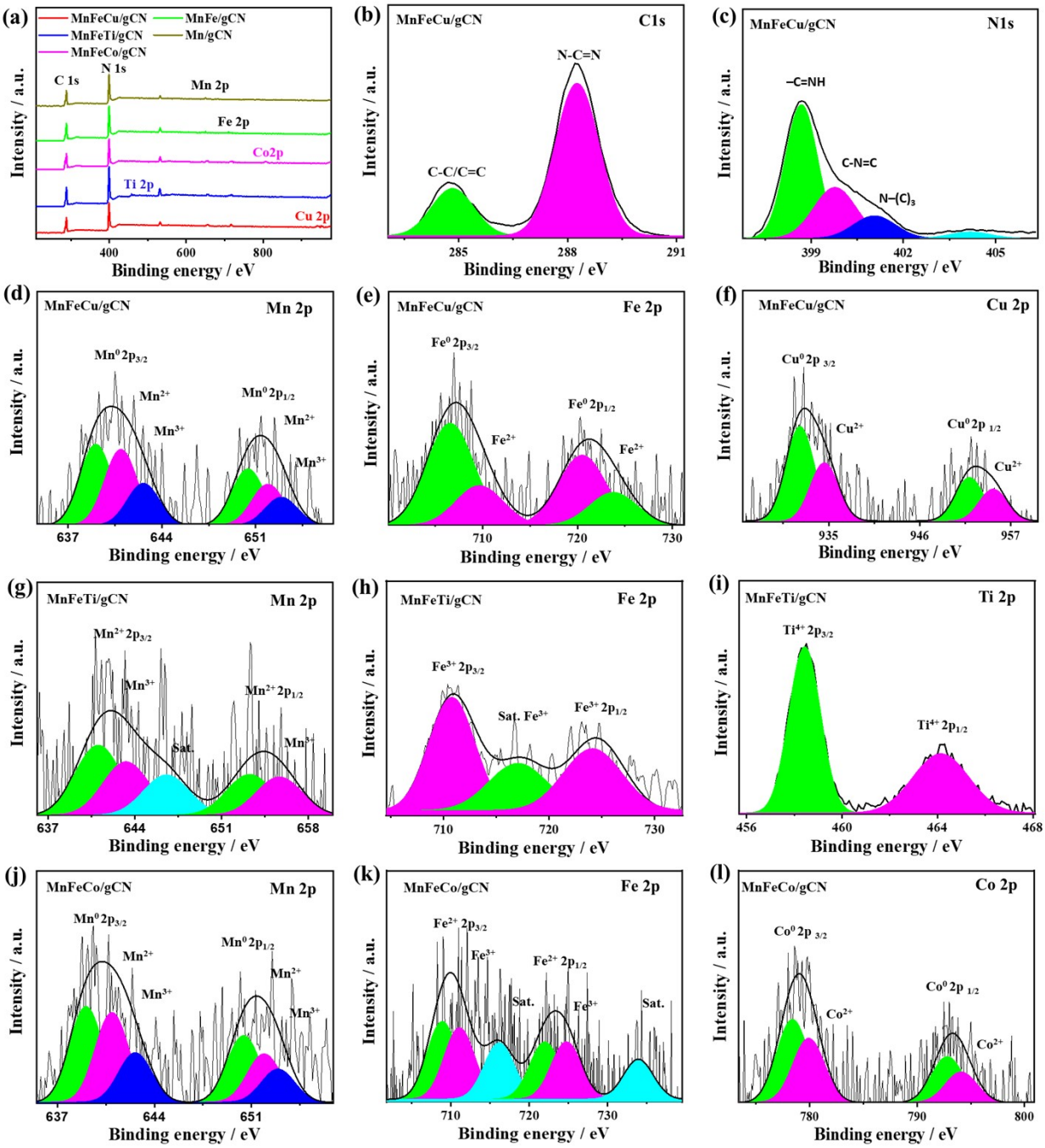

Figure 2. (a) XPS survey. High-resolution spectra of (b) C 1s, (c) N 1s of MnFeCu/g-C_3N_4. High-resolution spectra of Mn 2p, Fe 2p, and Cu 2p of (d-f) MnFeCu/g-C_3N_4, Mn 2p, Fe 2p, and Ti 2p of (g-i) MnFeTi/g-C_3N_4, and Mn 2p, Fe 2p, and Cu 2p of (j-l) MnFeCo/g-C_3N_4

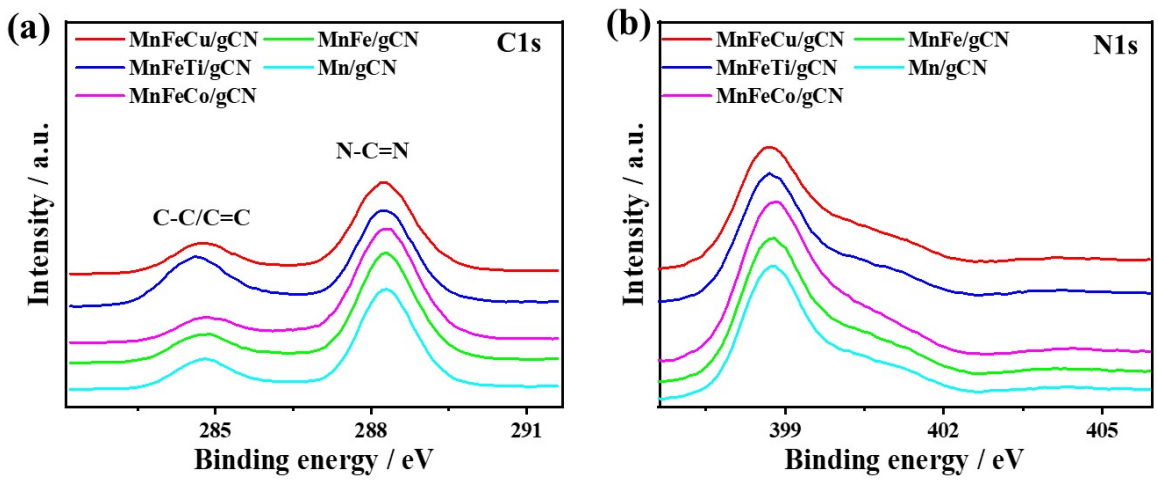

Figure S3. High-resolution XPS of (a) C1s (b) N1s.

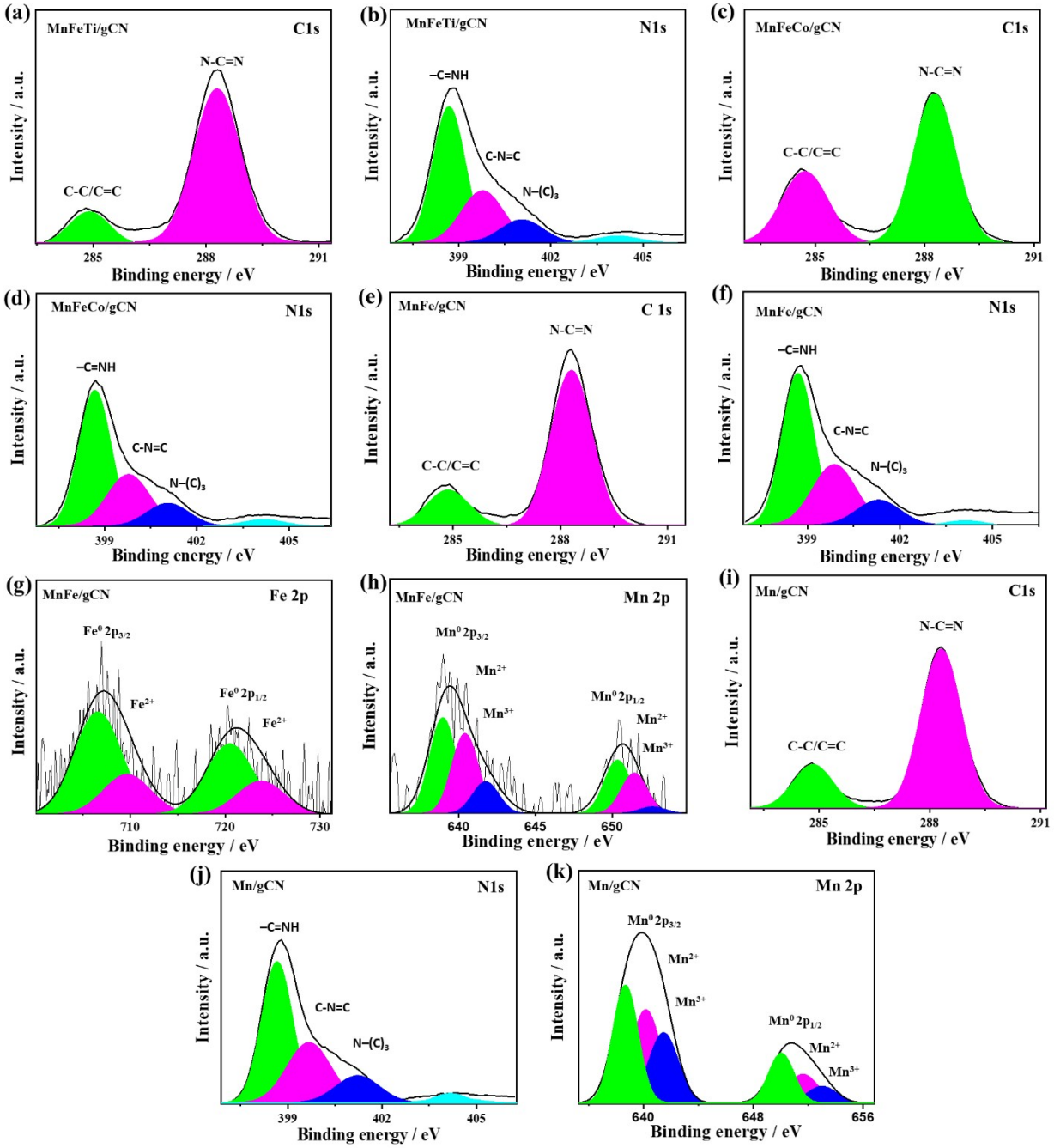

Figure S4. High-resolution XPS fitting of C 1s, N 1s (a-b) MnFeTi-gC_3N_4, (c-d) MnFeCo-gC_3N_4. (e-h) High-resolution XPS fitting of C 1s, N 1s, Mn 2p, and Fe 2p for MnFe-gC_3N_4. (e-h) High-resolution XPS fitting of C 1s, N 1s, and Mn 2p for Mn-gC_3N_4.

Table S2 Composition analysis of the as-formed materials.

catalyst	EDX (at.%)					ICP-OES (at.%)					XPS (at.%)				
	Mn	Fe	M	C	N	Mn	Fe	M	C	N	Mn	Fe	M	C	N
MnFeCu-gC_3N_4	0.65	0.61	0.74	41	57	0.55	0.49	0.7	41.16	57.1	0.55	0.51	0.64	41.2	57.1
MnFeTi-gC_3N_4	0.47	0.83	0.94	40.53	57.5	0.45	0.75	0.78	40.51	57.51	0.43	0.7	0.77	40.56	57.54
MnFeCo-gC_3N_4	0.72	0.8	0.77	40..41	57.3	0.64	0.72	0.69	40.61	57.34	0.62	0.71	0.67	40.61	57.39

MnFe-gC_3N_4	0.59	0.67	-	41.32	57.42	0.65	0.75	-	41.26	57.34	0.63	0.72	-	41.27	57.38
Mn-gC_3N_4	1.7	-	-	41.4	56.9	1.58	-	-	41.58	56.84	1.52	-	-	41.58	56.9

Table S3 The valance state and binding energies of the as-formed materials

Elements	**Mn^0 2p (eV)**		**Fe^0 2P (eV)**		**Cu^0 2p (eV)**		**Ti^0 2p (eV)**		**Co^0 2P (eV)**	
Catalyst	**2p 3/2**	**2p 1/2**	**2p 3/2**	**2p 1/2**	**2p 3/2**	**2p 1/2**	**2p 3/2**	**2p 1/2**	**2p 3/2**	**2p 1/2**
MnFeCo/g-C_3N_4	639.06	650.50	706.96	720.53	931.43	951.94	-	-	-	-
MnFeTi/g-C_3N_4	641.1 (Mn^{2+})	653.2 (Mn^{2+})	710.76 (Fe^{3+})	724.1 (Fe^{3+})	-	-	458.43 (Ti^{4+})	464.13 (Ti^{4+})	-	-
MnFeTi/g-C_3N_4	639.09	650.43	708.8 (Fe^{2+})	721.9 (Fe^{2+})	-	-	-	-	778.32	792.83
MnFe/g-C_3N_4	638.97	650.29	706.59	720.46	-	-	-	-	-	-
Mn/g-C_3N_4	638.71	650.04			-	-	-	-	-	-

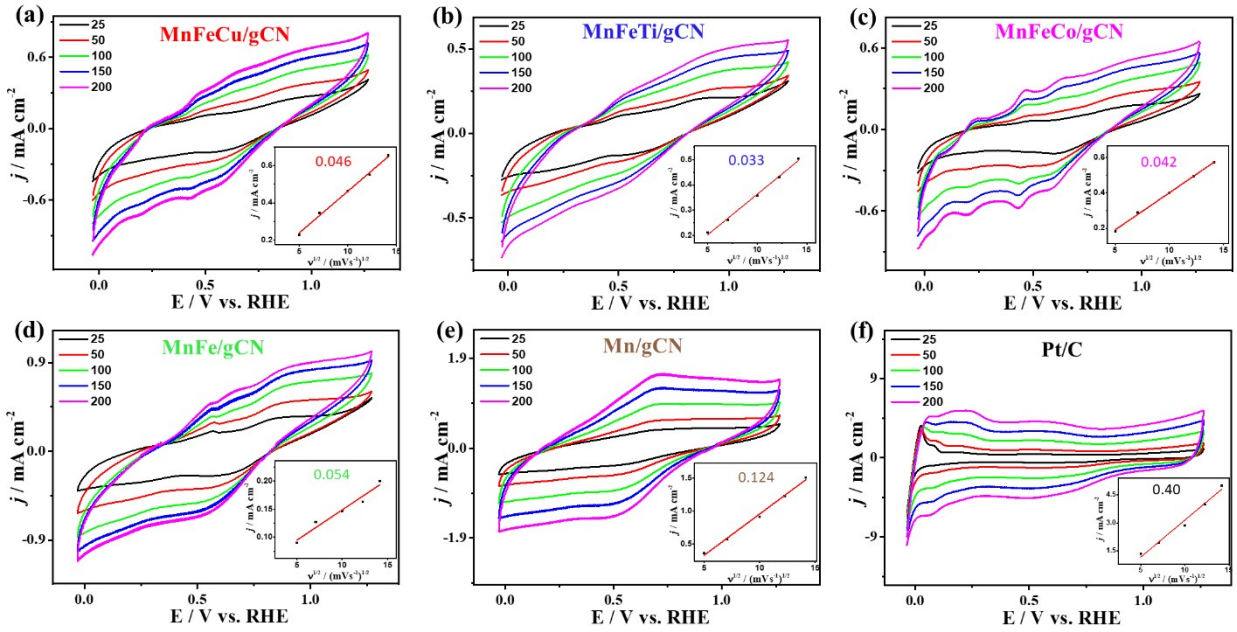

Figure S5. CV curves measured on the as-obtained catalysts at different scan rates and their related plots of *j* vs. $v^{1/2}$ in 0.5 M H_2SO_4

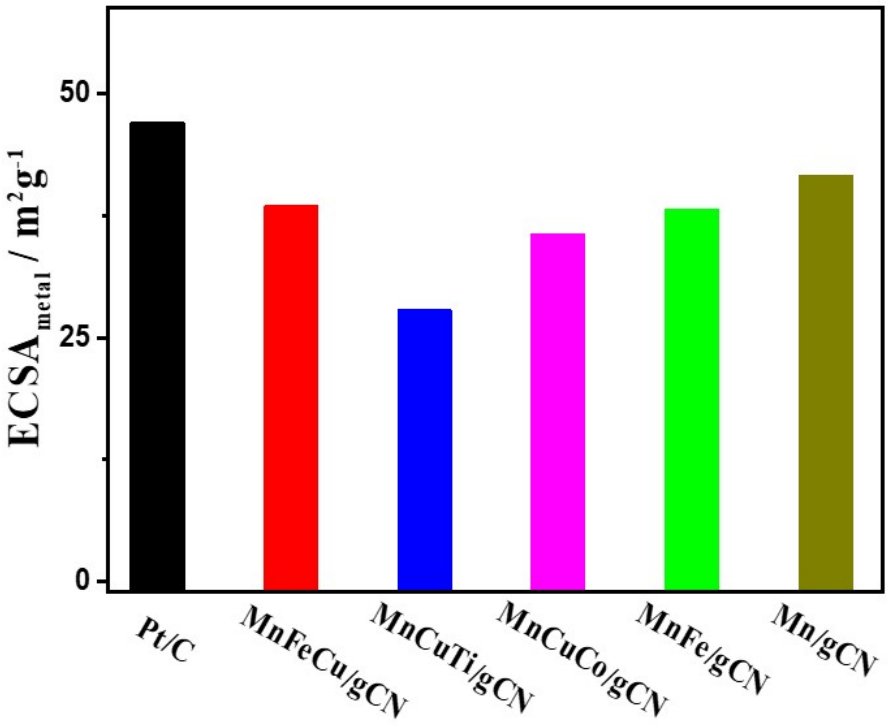

Figure S6. ECSA of the as-formed materials.

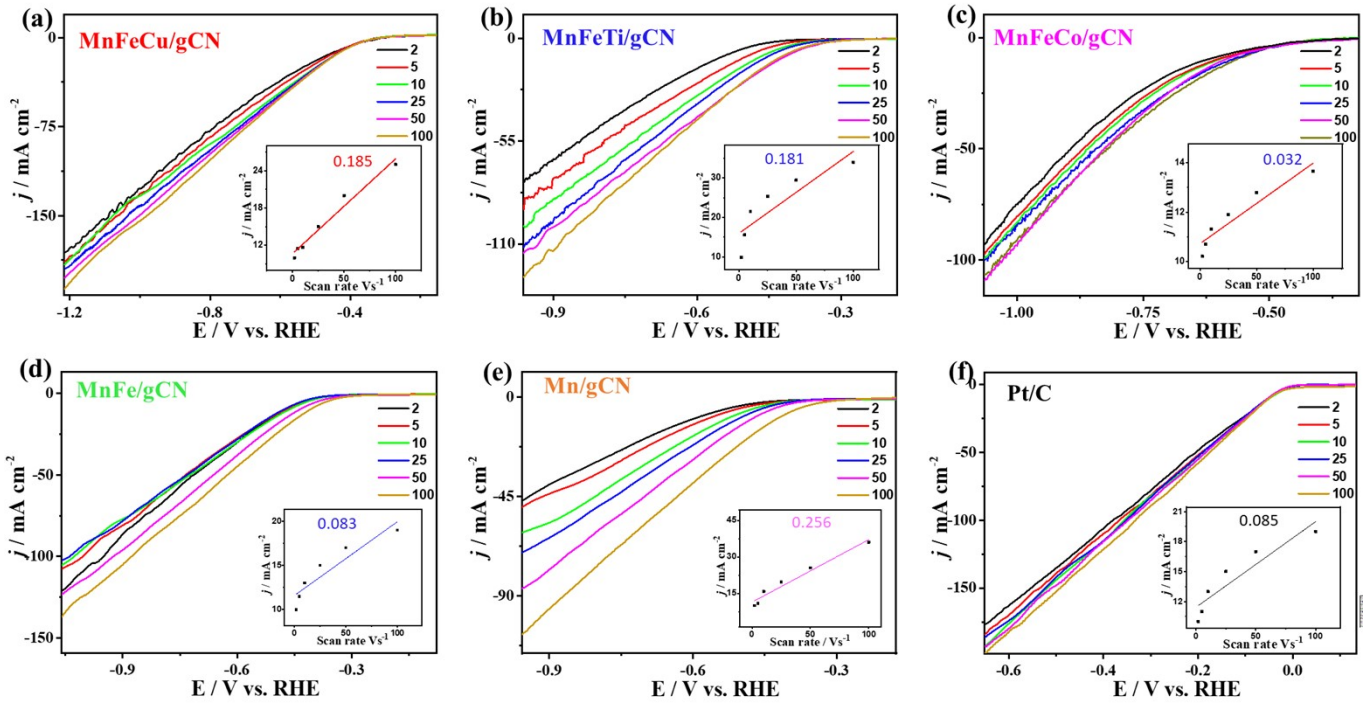

Figure S7. LSV measured at different scan rates tested on MnFeCu/g-C_3N_4, MnFeTi/g-C_3N_4, MnFeCo/g-C_3N_4, MnFe/g-C_3N_4, Mn/g-C_3N_4, and Pt/C catalyst in 0.5 M H_2SO_4 electrolyte.

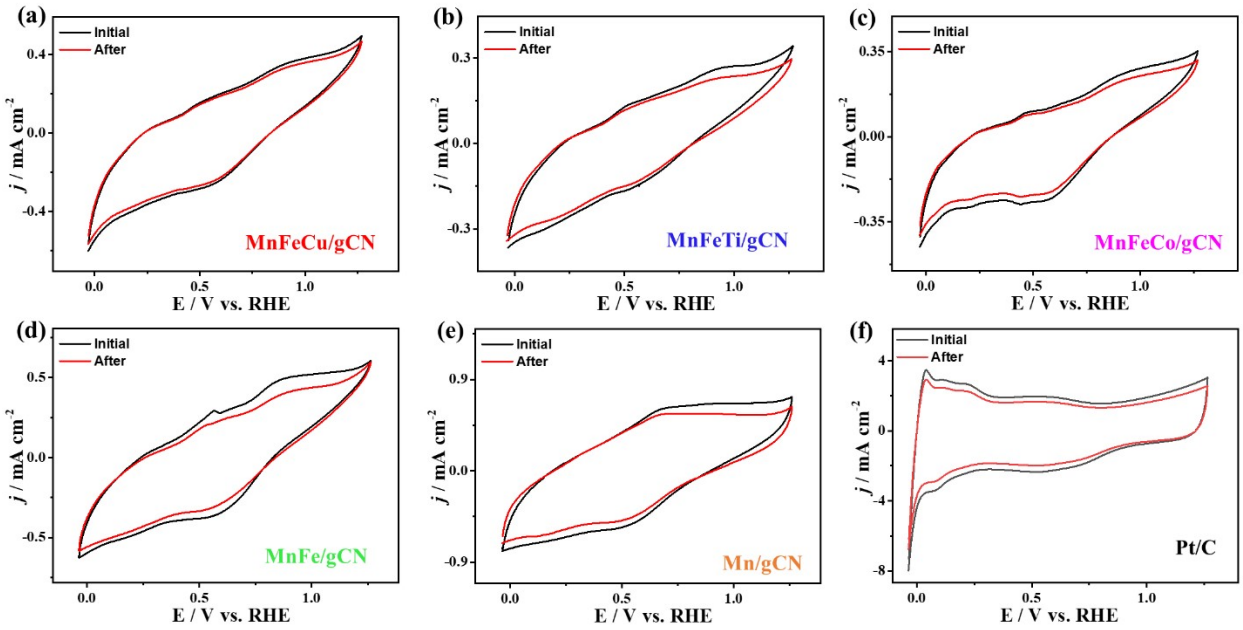

Figure S8. CV curve at scan rate 50 mV s^{-1} in 0.5 M H_2SO_4 purged with N_2 for catalysts before and after cyclic test.

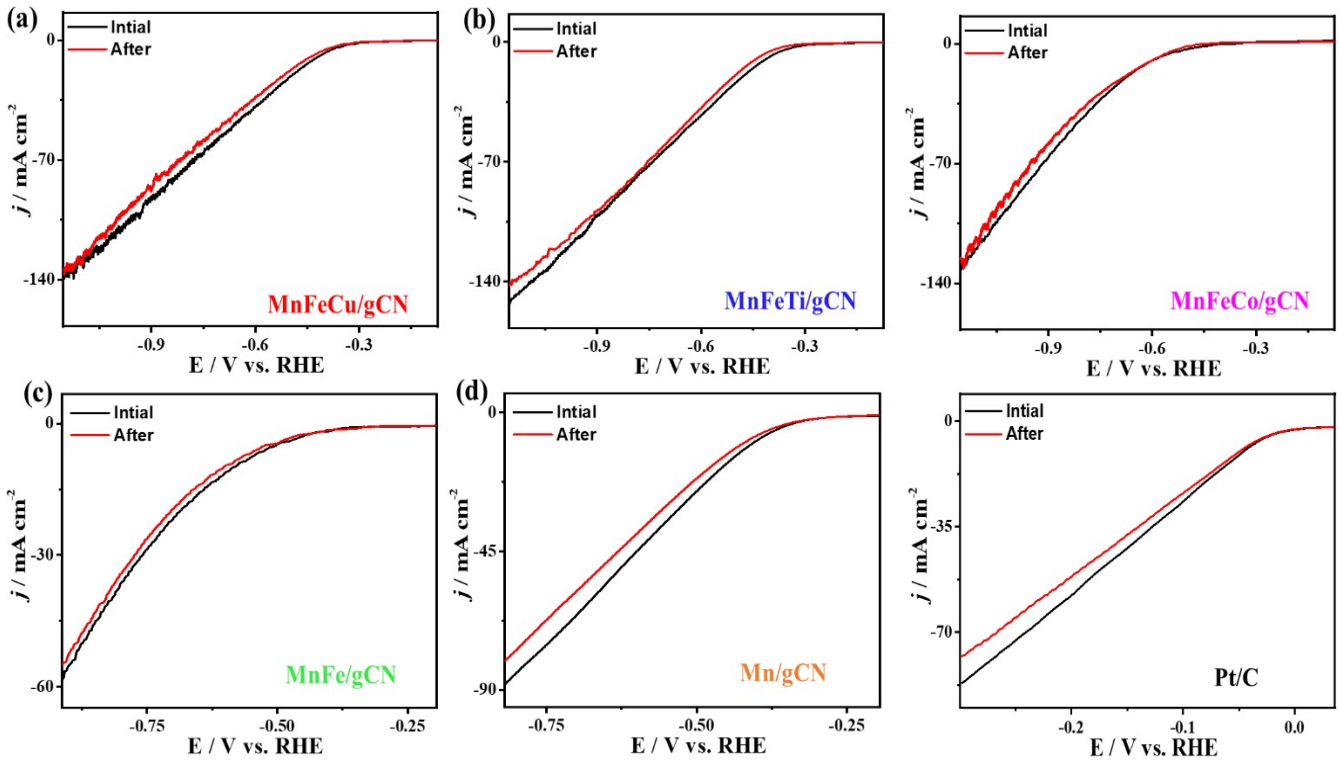

Figure 9. (a) (a) LSV before and after 1000 cycles measured at scan rate 2 mVs^{-1} tested on MnFeCu/g-C_3N_4, MnFeTi/g-C_3N_4, MnFeCo/g-C_3N_4, MnFe/g-C_3N_4, Mn/g-C_3N_4, and Pt/C catalyst in 0.5M H_2SO_4 electrolyte.

Table S4 Comparison of the HER activity of our developed MnFeCu/g-C_3N_4 and previous reported carbon-based catalysts in acidic electrolytes.

Catalyst	Onset Potential (V vs. RHE) (mV)	η10 (V vs. RHE)(mV)	Tafel slope [mV dec^{-1}]	TOF	Electrolyte	Ref.
MnFeCu/g-C_3N_4	-225	400	219	3.5	0.5 M H_2SO_4	This Work
N,P graphene-1	289	422	91	-	0.5 M H_2SO_4	[41]
NENU-501	150	397	137	-	0.5 M H_2SO_4	[42]
CTGU-6	349	425	176	-	0.5 M H_2SO_4	[43]
Cu-Pd/NPCC/HT/GCE	82	340	-	-	0.5 M H_2SO_4	[44]
N-doped graphene	-345	474	172	-	0.5 M H_2SO_4	[45]
5% F/BCN	-144	437	153	0.92	0.5 M H_2SO_4	[46]

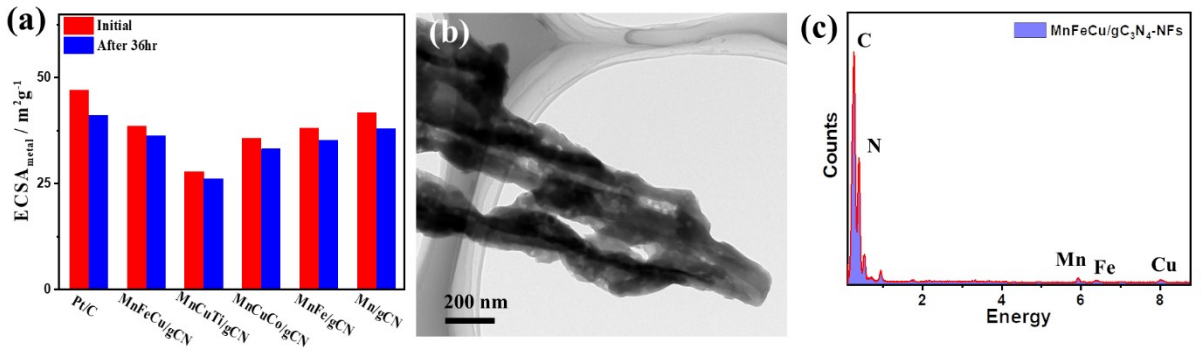

Figure S10. (a) ECSA before and after stability test , (b) TEM, and (c) EDX of MnFeCu/g-C_3N_4 after stability test.

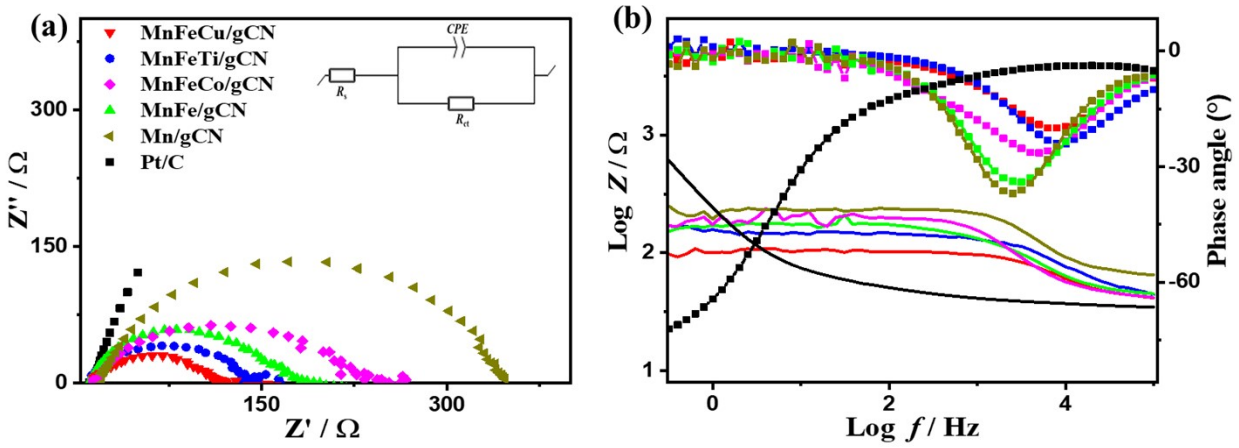

Figure S11. (a) Nyquist plots including (Voigt electrical equivalent circuit), and (b) Bode plots of MnFeCu/g-C_3N_4, MnFeTi/g-C_3N_4, MnFeCo/g-C_3N_4, MnFe/g-C_3N_4, Mn/g-C_3N_4, and Pt/C catalyst in 0.5 M H_2SO_4 electrolyte

Table S5 EIS fitting data of the as-made catalysts relative to Pt/C

Catalyst	R_s (Ω)	R_{ct} (Ω)	CPE (μF.$s^{(1-a)}$)	*a*

MnFeCu/g-C_3N_4NFs	41.4 ± 0.8	58 ± 0.15	1.94 ± 0.19	0.863 ± 0.013
MnFeTi/g-C_3N_4NFs	41.9 ± 1.3	265 ± 7.8	1.6 ± 0.695	0.851 ± 0.04
MnFeCo/g-C_3N_4NFs	43.8 ± 0.07	107 ± 0.2	1.13 ± 0.09	0.838± 0.015
MnFe/g-C_3N_4NFs	44 ± 0.023	159 ± 2.1	2 ± 0.003	894 ± 0.003
Mn/g-C_3N_4NFs	53.8 ± 1.69	132 ± 1.2	0.796 ± 27	0.801 ± 0.01
Pt/C (10 wt.%)	11.89 ± 0.06	171.1 ±	1.01 ±0.001	0.763 ± 0.02

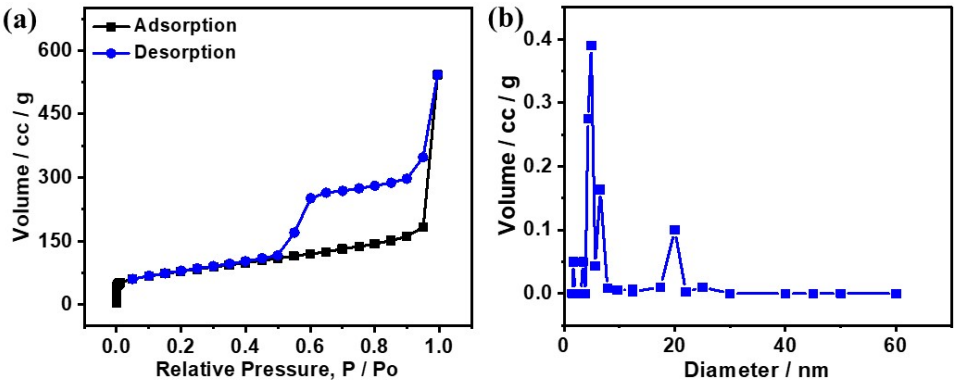

Figure S12. (a) N_2-physisorption isotherms and (b) pore size/volume of MnFeCu/g-C_3N_4. The N_2-physisorption isotherms were conducted on a Quantachrome Autosorb 3.01 instrument, and samples were degassed for 24 h at 50 °C under vacuum before the measurements.

References

1. K. Eid, M. H. Sliem, A. S. Eldesoky, H. Al-Kandari and A. M. Abdullah, *International Journal of Hydrogen Energy*, 2019, **44**, 17943-17953.
2. K. Eid, M. H. Sliem, K. Jlassi, A. S. Eldesoky, G. G. Abdo, S. Y. Al-Qaradawi, M. A. Sharaf, A. M. Abdullah and A. A. Elzatahry, *Inorganic Chemistry Communications*, 2019, **107**, 107460.
3. K. Eid, M. H. Sliem and A. M. Abdullah, *Nanoscale*, 2019, **11**, 11755-11764.
4. K. Eid, Y. H. Ahmad, A. T. Mohamed, A. G. Elsafy and S. Y. Al-Qaradawi, *Catalysts*, 2018, **8**, 411.
5. K. Eid, M. H. Sliem, H. Al-Kandari, M. A. Sharaf and A. M. Abdullah, *Langmuir*, 2019, **35**, 3421-3431.
6. K. Eid, M. H. Sliem, M. Al-Ejji, A. M. Abdullah, M. Harfouche and R. S. Varma, *ACS Applied Materials & Interfaces*, 2022, **14**, 40749-40760.
7. A. Abdelgawad, B. Salah, Q. Lu, A. M. Abdullah, M. Chitt, A. Ghanem, R. S. Al-Hajri and K. Eid, *Journal of Electroanalytical Chemistry*, 2023, **938**, 117426.
8. Y. Wang, X. Liu, J. Liu, B. Han, X. Hu, F. Yang, Z. Xu, Y. Li, S. Jia and Z. Li, *Angewandte Chemie*, 2018, **130**, 5867-5873.
9. Y. Zheng, L. Lin, X. Ye, F. Guo and X. Wang, *Angewandte Chemie*, 2014, **126**, 12120-12124.
10. X. Wang, C. Zhou, R. Shi, Q. Liu, G. I. Waterhouse, L. Wu, C.-H. Tung and T. Zhang, *Nano Research*, 2019, **12**, 2385-2389.
11. X. Fan, T. Wang, B. Gao, H. Gong, H. Xue, H. Guo, L. Song, W. Xia, X. Huang and J. He, *Langmuir*, 2016, **32**, 13322-13332.

12. Z. Yu, Y. Li, J. Qu, R. Zheng, J. M. Cairney, J. Zhang, M. Zhu, A. Khan and W. Li, *Chemical Engineering Journal*, 2021, **404**, 126458.
13. J. Sun, S. Yang, Z. Liang, X. Liu, P. Qiu, H. Cui and J. Tian, *Journal of colloid and interface science*, 2020, **567**, 300-307.
14. W. Peng, S.-S. Zhang, Y.-B. Shao and J.-H. Huang, *International Journal of Hydrogen Energy*, 2018, **43**, 22215-22225.
15. Z. Qin, F. Xue, Y. Chen, S. Shen and L. Guo, *Applied Catalysis B: Environmental*, 2017, **217**, 551-559.
16. T. Bhowmik, M. K. Kundu and S. Barman, *ACS applied materials & interfaces*, 2016, **8**, 28678-28688.
17. Y. Zhao, F. Zhao, X. Wang, C. Xu, Z. Zhang, G. Shi and L. Qu, *Angewandte Chemie International Edition*, 2014, **53**, 13934-13939.
18. K.-L. Chen, S.-S. Zhang, J.-Q. Yan, W. Peng, D.-P. Lei and J.-H. Huang, *International Journal of Hydrogen Energy*, 2019, **44**, 31916-31929.
19. J. Yang, Y. Liang, K. Li, G. Yang, K. Wang, R. Xu and X. Xie, *Catalysis Science & Technology*, 2019, **9**, 3342-3346.
20. X. Zhao, Y. Zhang, X. Zhao, X. Wang, Y. Zhao, H. Tan, H. Zhu, W. Ho, H. Sun and Y. Li, *ACS applied materials & interfaces*, 2019, **11**, 27934-27943.
21. J. Bai, Q. Han, Z. Cheng and L. Qu, *Chemistry–An Asian Journal*, 2018, **13**, 3160-3164.
22. Y. Wang, S. Zhao, Y. Zhang, J. Fang, W. Chen, S. Yuan and Y. Zhou, *ACS Sustainable Chemistry & Engineering*, 2018, **6**, 10200-10210.
23. G. Ge, X. Guo, C. Song and Z. Zhao, *ACS applied materials & interfaces*, 2018, **10**, 18746-18753.
24. Y. Gao, F. Hou, S. Hu, B. Wu, Y. Wang, H. Zhang, B. Jiang and H. Fu, *ChemCatChem*, 2018, **10**, 1330-1335.
25. Z. Sun, W. Wang, Q. Chen, Y. Pu, H. He, W. Zhuang, J. He and L. Huang, *Journal of Materials Chemistry A*, 2020, **8**, 3160-3167.
26. S. Guo, Z. Deng, M. Li, B. Jiang, C. Tian, Q. Pan and H. Fu, *Angewandte Chemie International Edition*, 2016, **55**, 1830-1834.
27. Z. Mo, H. Xu, Z. Chen, X. She, Y. Song, J. Wu, P. Yan, L. Xu, Y. Lei and S. Yuan, *Applied Catalysis B: Environmental*, 2018, **225**, 154-161.
28. G. Zhang, A. Savateev, Y. Zhao, L. Li and M. Antonietti, *Journal of Materials Chemistry A*, 2017, **5**, 12723-12728.
29. Y. Zhu, A. Marianov, H. Xu, C. Lang and Y. Jiang, *ACS applied materials & interfaces*, 2018, **10**, 9468-9477.
30. Z. Huang, F. Li, B. Chen and G. Yuan, *RSC advances*, 2015, **5**, 102700-102706.
31. D. Long, W. Chen, S. Zheng, X. Rao and Y. Zhang, *Industrial & Engineering Chemistry Research*, 2020, **59**, 4549-4556.
32. H. Li, X. Bao, Z. Wang, Z. Zheng, P. Wang, Y. Liu, X. Zhang, X. Qin, Y. Dai and Y. Li, *International Journal of Hydrogen Energy*, 2019, **44**, 28780-28788.
33. S. Guo, Y. Tang, Y. Xie, C. Tian, Q. Feng, W. Zhou and B. Jiang, *Applied Catalysis B: Environmental*, 2017, **218**, 664-671.
34. X. Liu, X. Wu, D. Long, X. Rao and Y. Zhang, *Journal of Photochemistry and Photobiology A: Chemistry*, 2020, **391**, 112337.
35. G. Ge and Z. Zhao, *Catalysis Science & Technology*, 2019, **9**, 266-270.
36. W. Wang, Z. Shu, J. Zhou, T. Li, P. Duan, Z. Zhao, Y. Tan, C. Xie and S. Cui, *Applied Clay Science*, 2018, **158**, 143-149.
37. S. Kang, J. Jang, S.-h. Ahn and C. S. Lee, *Dalton Transactions*, 2019, **48**, 2170-2178.

38. J. Zhang, M. Wu, B. He, R. Wang, H. Wang and Y. Gong, *Applied Surface Science*, 2019, **470**, 565-572.
39. Y. Zeng, X. Liu, C. Liu, L. Wang, Y. Xia, S. Zhang, S. Luo and Y. Pei, *Applied Catalysis B: Environmental*, 2018, **224**, 1-9.
40. P. Wang, I. Sinev, F. Sun, H. Li, D. Wang, Q. Li, X. Wang, R. Marschall and M. Wark, *RSC Advances*, 2017, **7**, 42774-42782.
41. Y. Zheng, Y. Jiao, L. H. Li, T. Xing, Y. Chen, M. Jaroniec and S. Z. J. A. n. Qiao, 2014, **8**, 5290-5296.
42. J.-S. Qin, D.-Y. Du, W. Guan, X.-J. Bo, Y.-F. Li, L.-P. Guo, Z.-M. Su, Y.-Y. Wang, Y.-Q. Lan and H.-C. J. J. o. t. A. C. S. Zhou, 2015, **137**, 7169-7177.
43. Y. P. Wu, W. Zhou, J. Zhao, W. W. Dong, Y. Q. Lan, D. S. Li, C. Sun and X. J. A. C. Bu, 2017, **129**, 13181-13185.
44. S. Mandegarzad, J. B. Raoof, S. R. Hosseini and R. J. A. S. S. Ojani, 2018, **436**, 451-459.
45. Y. Ito, W. Cong, T. Fujita, Z. Tang and M. J. A. C. I. E. Chen, 2015, **54**, 2131-2136.
46. M. A. Ahsan, T. He, K. Eid, A. M. Abdullah, M. L. Curry, A. Du, A. R. Puente Santiago, L. Echegoyen and J. C. J. J. o. t. A. C. S. Noveron, 2021, **143**, 1203-1215.